



# A Sensitive Search for Supernova Emission Associated with the Extremely Energetic and Nearby GRB 221009A

Gokul P. Srinivasaragavan<sup>1,2,3</sup> , Brendan O'Connor<sup>1,3,4,5</sup> , S. Bradley Cenko<sup>2,3</sup> , Alexander J. Dittmann<sup>1,2</sup> , Sheng Yang<sup>6,7</sup> , Jesper Sollerman<sup>7</sup> , G. C. Anupama<sup>8</sup> , Sudhanshu Barway<sup>8</sup> , Varun Bhalerao<sup>9</sup> , Harsh Kumar<sup>9</sup> , Vishwajeet Swain<sup>9</sup> , Erica Hammerstein<sup>1,3,10</sup> , Isiah Holt<sup>1,2,3</sup> , Shreya Anand<sup>11</sup> , Igor Andreoni<sup>1,2,3,25</sup> , Michael W. Coughlin<sup>12</sup> , Simone Dichiara<sup>13</sup> , Avishay Gal-Yam<sup>14</sup> , M. Coleman Miller<sup>1,2</sup> , Jaime Soon<sup>15</sup> , Roberto Soria<sup>16,17,18</sup> , Joseph Durbak<sup>3,10,19</sup> , James H. Gillanders<sup>20</sup> , Sibasish Laha<sup>3,10,21</sup> , Anna M. Moore<sup>22</sup> , Fabio Ragosta<sup>23</sup> , and Eleonora Troja<sup>20,24</sup>

<sup>1</sup> Department of Astronomy, University of Maryland, College Park, MD 20742, USA; [gusriniv2@umd.edu](mailto:gusriniv2@umd.edu)

<sup>2</sup> Joint Space-Science Institute, University of Maryland, College Park, MD 20742, USA

<sup>3</sup> Astrophysics Science Division, NASA Goddard Space Flight Center, 8800 Greenbelt Rd, Greenbelt, MD 20771, USA

<sup>4</sup> Department of Physics, The George Washington University, Washington, DC 20052, USA

<sup>5</sup> Astronomy, Physics and Statistics Institute of Sciences (APSS), The George Washington University, Washington, DC 20052, USA

<sup>6</sup> Henan Academy of Sciences, Zhengzhou 450046, Henan, People's Republic of China

<sup>7</sup> Department of Astronomy, The Oskar Klein Center, Stockholm University, AlbaNova, SE-10691 Stockholm, Sweden

<sup>8</sup> Indian Institute of Astrophysics, 2nd Block 100 Feet Rd, Koramangala Bangalore 560 034, India

<sup>9</sup> Department of Physics, Indian Institute of Technology Bombay, Powai 400 076, India

<sup>10</sup> Center for Research and Exploration in Space Science and Technology, NASA/GSFC, Greenbelt, MD 20771, USA

<sup>11</sup> Division of Physics, Mathematics and Astronomy, California Institute of Technology, Pasadena, CA 91125, USA

<sup>12</sup> School of Physics and Astronomy, University of Minnesota, Minneapolis, MN 55455, USA

<sup>13</sup> Department of Astronomy and Astrophysics, The Pennsylvania State University, 525 Davey Lab, University Park, PA 16802, USA

<sup>14</sup> Department of Particle Physics and Astrophysics, Weizmann Institute of Science, 76100 Rehovot, Israel

<sup>15</sup> Research School of Astronomy and Astrophysics, Australian National University, Cotter Rd, Weston Creek, ACT 2611, Australia

<sup>16</sup> College of Astronomy and Space Sciences, University of the Chinese Academy of Sciences, Beijing 100049, People's Republic of China

<sup>17</sup> INAF—Osservatorio Astrofisico di Torino, Strada Osservatorio 20, I-10025 Pino Torinese, Italy

<sup>18</sup> Sydney Institute for Astronomy, School of Physics A28, The University of Sydney, NSW 2006, Australia

<sup>19</sup> Department of Physics, University of Maryland, College Park, MD 20742, USA

<sup>20</sup> Department of Physics, University of Rome “Tor Vergata, via della Ricerca Scientifica 1, I-00133 Rome, Italy

<sup>21</sup> Center for Space Science and Technology, University of Maryland Baltimore County, 1000 Hilltop Circle, Baltimore, MD 21250, USA

<sup>22</sup> Australian National University, Research School of Astronomy and Astrophysics, Mount Stromlo Observatory, Cotter Road, Weston Creek 2611, Australia

<sup>23</sup> INAF, Osservatorio Astronomico di Roma, via Frascati 33, I-00078 Monte Porzio Catone (RM), Italy

<sup>24</sup> INAF—Istituto di Astrofisica e Planetologia Spaziali, via Fosso del Cavaliere 100, I-00133 Rome, Italy

Received 2023 March 22; revised 2023 April 18; accepted 2023 April 23; published 2023 June 5

## Abstract

We report observations of the optical counterpart of the long gamma-ray burst GRB 221009A. Due to the extreme rarity of being both nearby ( $z = 0.151$ ) and highly energetic ( $E_{\gamma, \text{iso}} \geq 10^{54}$  erg), GRB 221009A offers a unique opportunity to probe the connection between massive star core collapse and relativistic jet formation across a very broad range of  $\gamma$ -ray properties. Adopting a phenomenological power-law model for the afterglow and host galaxy estimates from high-resolution Hubble Space Telescope imaging, we use Bayesian model comparison techniques to determine the likelihood of an associated supernova (SN) contributing excess flux to the optical light curve. Though not conclusive, we find moderate evidence ( $K_{\text{Bayes}} = 10^{1.2}$ ) for the presence of an additional component arising from an associated SN, SN 2022xiw, and find that it must be substantially fainter ( $<67\%$  as bright at the 99% confidence interval) than SN 1998bw. Given the large and uncertain line-of-sight extinction, we attempt to constrain the SN parameters ( $M_{\text{Ni}}$ ,  $M_{\text{ej}}$ , and  $E_{\text{KE}}$ ) under several different assumptions with respect to the host galaxy's extinction. We find properties that are broadly consistent with previous GRB-associated SNe:  $M_{\text{Ni}} = 0.05\text{--}0.25 M_{\odot}$ ,  $M_{\text{ej}} = 3.5\text{--}11.1 M_{\odot}$ , and  $E_{\text{KE}} = (1.6\text{--}5.2) \times 10^{52}$  erg. We note that these properties are weakly constrained due to the faintness of the SN with respect to the afterglow and host emission, but we do find a robust upper limit on  $M_{\text{Ni}}$  of  $M_{\text{Ni}} < 0.36 M_{\odot}$ . Given the tremendous range in isotropic gamma-ray energy release exhibited by GRBs (seven orders of magnitude), the SN emission appears to be decoupled from the central engine in these systems.

*Unified Astronomy Thesaurus concepts:* Core-collapse supernovae (304); Gamma-ray bursts (629); Relativistic jets (1390)

## 1. Introduction

Over the past two and a half decades, a link has been established between long-duration gamma-ray bursts (LGRBs) and core-collapse supernovae (CCSNe; Woosley & Bloom 2006). Over two dozen LGRBs have been associated with CCSNe, either indirectly (e.g., through late-time “bumps” in their optical afterglow light curves), or directly through telltale spectroscopic signatures (Cano et al. 2017). All of these

<sup>25</sup> Gehrels Fellow.

SNe are of the Ic-BL type (Filippenko 1997): they lack H and He lines in their optical spectra, and possess broad lines (BLs) indicative of higher ejecta velocities than seen in normal Type Ic SNe.

Despite this progress, a number of key open questions regarding the nature of the GRB-SN connection remain. One of the foremost of these is understanding why a much smaller fraction of Type Ic-BL SNe have associated LGRBs than the converse. A number of studies (Soderberg et al. 2006; Corsi et al. 2016, 2022) have shown that this dichotomy cannot be explained solely by viewing angle effects, and that relativistic ejecta are not ubiquitous to SNe Ic-BL (<19% of Ic-BL events are SN 1998bw-like, the prototypical SN associated with a GRB; Corsi et al. 2022). Therefore, there are intrinsic differences in the explosion mechanisms and/or environments between jet-powered Type Ic-BL SNe and normal Ic-BL events, and understanding this dichotomy can provide important insights into stellar evolution and the landscape of stellar explosions.

The observed population of LGRBs is comprised predominantly of cosmological ( $z \gtrsim 1$ ) events, with  $E_{\gamma, \text{iso}}$  between  $10^{50}$  and  $10^{54}$  erg (e.g., Jakobsson et al. 2006). On the other hand, the majority of GRBs that have associated spectroscopically confirmed SNe (GRB-SNe) are low-luminosity events, with isotropic-equivalent energies ( $E_{\gamma, \text{iso}}$ ) between  $10^{48}$  and  $10^{50}$  erg (Cano et al. 2017). This is the natural consequence of low-luminosity GRBs dominating the population of events nearby enough for spectroscopic investigations ( $z \lesssim 0.3$ ), even with large-aperture optical facilities. Here we attempt to characterize the SN associated with a rare energetic LGRB discovered in the nearby universe.

GRB 221009A [ $\alpha$  (J2000) =  $19^{\text{h}}13^{\text{m}}03^{\text{s}}.50$ ,  $\delta$  (J2000) =  $+19^{\circ}46'24''.23$ ; Laskar et al. 2022] was discovered by the Burst Alert Telescope (BAT; Barthelmy et al. 2005) on the Neil Gehrels Swift Observatory (Swift; Gehrels et al. 2004), though initially classified as a potential Galactic transient (Dichiara et al. 2022). Subsequently, the Fermi Gamma-Ray Burst Monitor (GBM; Meegan et al. 2009) reported an extremely bright LGRB detected  $\approx 55$  minutes earlier<sup>26</sup> consistent with this localization (Lesage et al. 2022). Further observations revealed that the BAT triggered on the bright X-ray afterglow of GRB 221009A, a first in the nearly 18 yr of Swift operations (Williams et al. 2023).

The unprecedented brightness led to extensive follow up across the electromagnetic spectrum (e.g., Fulton et al. 2023; Laskar et al. 2023; Kann et al. 2023; O’Connor et al. 2023; Williams et al. 2023). Spectroscopy of the optical afterglow led to a redshift measurement of  $z = 0.151$  (de Ugarte Postigo et al. 2022a; Castro-Tirado et al. 2022; Malesani et al. 2023). Its associated gamma-ray isotropic energy release is well in excess of  $10^{54}$  erg, making GRB 221009A an extremely rare example of a highly energetic LGRB nearby enough to search for an associated SN Ic-BL.

In this *Letter*, we present optical observations that display a late-time flattening in the afterglow decay of GRB 221009A, and we investigate how these measurements can constrain the possible associated SN (SN 2022xiw; de Ugarte Postigo et al. 2022c). In Section 2 we report the observations of the optical afterglow of GRB 221009A; in Section 3 we analyze the observations, and statistically compare models with and

without a SN component; in Section 4 we constrain the physical parameters of SN 2022xiw; in Section 5 we place GRB 221009A/SN 2022xiw in the context of the GRB-SN sample in the literature; and in Section 6 we summarize our conclusions. In the final stages of manuscript preparation, studies reporting conflicting results on the existence of SN emission were posted on the arXiv (Fulton et al. 2023; Kann et al. 2023; Levan et al. 2023; Shrestha et al. 2023)—where relevant we highlight differences in our approach and contrasts in our results.

## 2. Observations

The main telescopes used for this work are the GROWTH-India Telescope (GIT), Lowell Discovery Telescope (LDT), and the Gemini-South Telescope. The results of the GIT, LDT, and Gemini-South observations are presented in Table 1. To provide additional coverage at early times and help constrain the afterglow behavior, we have also considered optical afterglow measurements from the Liverpool Telescope (LT) reported in Laskar et al. (2023), and supplemented these with preliminary results reported in the GCN circulars (Belkin et al. 2022a, 2022b, 2022; Bikmaev et al. 2022a, 2022b; Brivio et al. 2022; D’Avanzo et al. 2022; de Wet & Groot 2022; Ferro et al. 2022; Groot et al. 2022; Gupta et al. 2022; Huber et al. 2022; Im et al. 2022; Izzo et al. 2022; Kim et al. 2022; Kumar et al. 2022a; Pellegrin et al. 2022; Rajabov et al. 2022; Rossi et al. 2022; Schneider et al. 2022; Shrestha et al. 2022; Vinko et al. 2022). The GCN photometry is provided in tabular form in Table 4. All times used in this work are in the observer frame. Below we describe the data reduction processes for each of the telescopes we use.

### 2.1. GIT

We used the GIT located at the Indian Astronomical Observatory (IAO), Hanle-Ladakh, to acquire observations of the GRB 221009A optical afterglow (Kumar et al. 2022b). The source was observed in Sloan  $g'$ ,  $r'$ ,  $i'$ , and  $z'$  bands. Data were downloaded and processed in real time by the GIT data reduction pipeline. We used individual exposures for photometry in the early stages when the afterglow was bright. Later, we stacked images with SWarp (Bertin 2010) to increase the signal-to-noise ratio (S/N) of the detections.

The data were reduced in a standard manner using the GIT pipeline (Kumar et al. 2022c). All images were preprocessed by subtracting bias, flat fielding, and cosmic-ray removal via the Astro-SCRAPPY (McCully & Tewes 2019) package. Astrometry was performed on the resulting images using the offline solve-field astrometry engine. Sources were detected using SExtractor (Bertin & Arnouts 1996) and were cross-matched against the Pan-STARRS1 DR1 catalog (PS1; Flewelling et al. 2020) through Vizier to obtain the zero-point. Finally, the pipeline performed point-spread function (PSF) fit photometry to obtain the magnitudes of the GRB 221009A afterglow (Table 1).

### 2.2. LDT

We also observed GRB 221009A in  $r'$ ,  $i'$ , and  $z'$  with the 4.3 m Large Monolithic Imager (LMI) on the LDT through an approved Target-of-Opportunity (ToO) program. We reduced the images using a custom Python-based image analysis pipeline (Toy et al. 2016), that can perform data reduction,

<sup>26</sup> At 13:16:59.00 UTC on 2022 October 9, which we establish hereafter as  $T_0$ .

**Table 1**

Optical Photometry and Associated  $1\sigma$  Errors of GRB 221009A, Which Includes Contributions From its Afterglow, Host Galaxy, and Associated SN 2022xiw

$t_{\text{obs}} - T_0$ (days)	Telescope	Filter	AB mag	Uncertainty
0.12835635	GIT	$g'$	17.66	0.08
0.13105835	GIT	$r'$	16.16	0.07
0.13366335	GIT	$i'$	15.17	0.03
0.13633535	GIT	$z'$	14.50	0.04
0.14391035	GIT	$g'$	17.69	0.07
0.14653335	GIT	$r'$	16.26	0.05
0.14922235	GIT	$i'$	15.28	0.03
0.15183035	GIT	$z'$	14.57	0.05
0.15955335	GIT	$g'$	17.99	0.10
0.16225435	GIT	$r'$	16.32	0.05
0.16486235	GIT	$i'$	15.34	0.04
0.16755835	GIT	$z'$	14.64	0.06
0.17138035	GIT	$g'$	17.94	0.11
0.17407535	GIT	$r'$	16.40	0.05
0.17668335	GIT	$i'$	15.41	0.04
0.17939935	GIT	$z'$	14.71	0.07
0.18711135	GIT	$g'$	18.11	0.16
0.18971935	GIT	$r'$	16.49	0.05
0.19239635	GIT	$i'$	15.47	0.05
0.19499735	GIT	$z'$	14.72	0.06
1.03149435	GIT	$g'$	20.21	0.23
1.03551335	GIT	$z'$	16.75	0.05
1.03843935	GIT	$z'$	16.73	0.06
1.04287735	GIT	$i'$	17.48	0.04
1.04447835	GIT	$i'$	17.49	0.03
1.04607935	GIT	$i'$	17.52	0.04
1.05022335	GIT	$r'$	18.58	0.06
1.05371835	GIT	$r'$	18.55	0.05
1.08636135	GIT	$g'$	20.50	0.16
1.09184435	GIT	$z'$	16.90	0.15
1.10147035	GIT	$r'$	18.66	0.08
1.14527035	GIT	$z'$	17.06	0.08
1.14817435	GIT	$z'$	17.01	0.15
2.11955235	GIT	$r'$	19.77	0.14
2.14304035	GIT	$z'$	17.99	0.15
3.00313235	GIT	$i'$	19.20	0.14
3.00693735	GIT	$r'$	20.41	0.15
3.00697835	GIT	$z'$	18.57	0.16
4.02688035	GIT	$i'$	19.68	0.14
4.03068335	GIT	$r'$	20.83	0.16
4.03069335	GIT	$z'$	18.82	0.17
5.07656435	GIT	$r'$	20.91	0.21
5.07656635	GIT	$i'$	19.85	0.19
5.08403035	GIT	$z'$	18.93	0.17
6.09907835	GIT	$i'$	20.43	0.18
6.10467335	GIT	$z'$	19.41	0.19
3.6	LDT	$g'$	22.06	0.04
3.6	LDT	$r'$	20.44	0.04
3.6	LDT	$i'$	19.37	0.01
3.6	LDT	$z'$	18.67	0.01
9.5	LDT	$r'$	21.5	0.08
9.5	LDT	$i'$	20.75	0.05
9.5	LDT	$z'$	20.01	0.03
18.5	LDT	$g'$	24.71	0.15
18.5	LDT	$r'$	22.71	0.06
18.5	LDT	$i'$	21.83	0.15
18.5	LDT	$z'$	20.97	0.05
21.5	LDT	$r'$	22.91	0.06
21.5	LDT	$i'$	21.82	0.02
21.5	LDT	$z'$	21.37	0.04
28.5	LDT	$r'$	23.55	0.15
28.5	LDT	$i'$	22.07	0.09
28.5	LDT	$z'$	21.45	0.07

**Table 1**

(Continued)

$t_{\text{obs}} - T_0$ (days)	Telescope	Filter	AB mag	Uncertainty
36.53	LDT	$r'$	23.64	0.11
36.53	LDT	$i'$	22.45	0.05
36.53	LDT	$z'$	21.82	0.07
52.53	LDT	$i'$	22.73	0.15
4.4	Gemini-South	$i'$	19.78	0.02
17.4	Gemini-South	$i'$	21.71	0.05

**Note.** All times are in the observer frame. The magnitudes are not corrected for Galactic extinction.

astrometry, registration, source extraction, and PSF photometry using `SExtractor`, which was calibrated using point sources from the PS1 catalog (Table 1). These observations were also reported in O'Connor et al. (2022a, 2022b, 2023). Figure 1 shows both the wider field of view of GRB 221009A's position on the sky, as well as the individual evolution of its flux over time in both filters.

### 2.3. Gemini-South

Two additional publicly available  $i'$ -band observations obtained with GMOS-S mounted on the 8.1 m Gemini-South Telescope (PIs: Rastinejad, O'Connor; Rastinejad & Fong 2022) were also analyzed. The data were reduced using DRAGONS<sup>27</sup> (Labrie et al. 2019) to align and stack individual frames. PSF photometry was calibrated using nearby point sources in the PS1 catalog (Table 1).

## 3. Analysis and Model Selection

### 3.1. Previous Broadband Modeling Results

We draw upon three results from previous studies of the broadband afterglow of GRB 221009A in order to inform our approach to characterizing the associated SN emission. First, fits to the broadband spectral energy distribution (SED) revealed that the frequency range from optical to hard X-rays is not well fit by a single power law (i.e.,  $f_\nu \propto \nu^{-\beta}$ ). Instead, a change in the spectral slope, physically attributed to the synchrotron cooling frequency ( $\nu_c$ ), is inferred around the X-ray bandpass (O'Connor et al. 2023; Williams et al. 2023). As a result, in standard synchrotron afterglow theory, we do not expect the optical afterglow to decay with the same power-law index as the X-rays (e.g., Sari et al. 1998). Thus, to remove the afterglow contribution we must model the optical decay separately from the X-rays (see Fulton et al. 2023 and the first approach in Shrestha et al. 2023).

Second, in addition to significant extinction due to dust in the Milky Way galaxy, broadband SED fits indicate the possible existence of absorption beyond the nominal value of  $E(B - V) = 1.30$  mag reported in Schlafly & Finkbeiner (2011). Given the low redshift, it is difficult to disentangle a larger than expected Galactic extinction (e.g., due to small-scale variations in Galactic dust), or extinction in the GRB host galaxy. Existing works differ on the significance of this extinction component, with inferred values ranging from  $E(B - V) = 1.30$  mag (i.e., no additional extinction; O'Connor et al. 2023) to

<sup>27</sup> <https://dragons.readthedocs.io/>

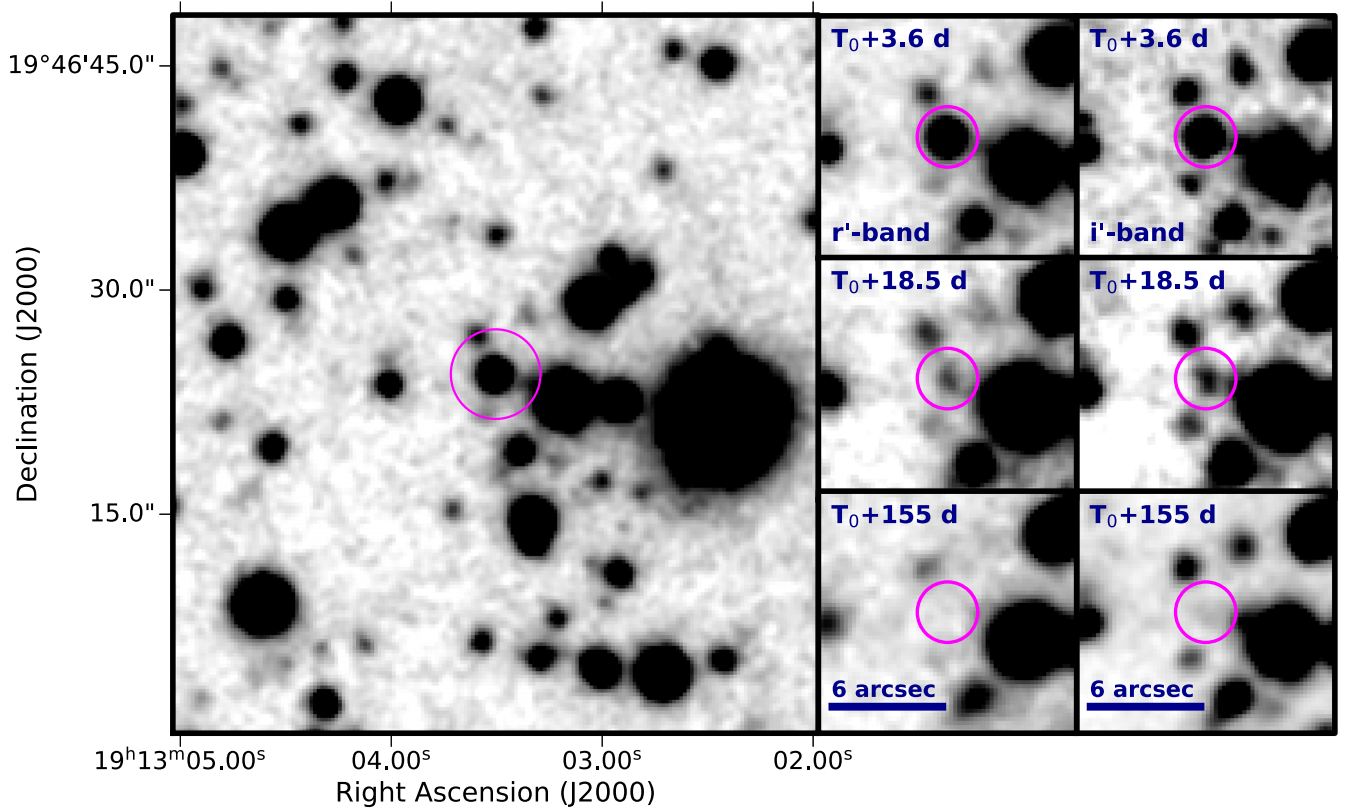


**Figure 1.** LDT images of the optical afterglow of GRB 221009A. All of the panels show the position of GRB 221009A circled in pink. The left, large panel shows the wider field of view of GRB 221009A, in  $r'$  band 3.6 days after  $T_0$ . The right panels show the evolution over time of the optical afterglow, in both the  $r'$  and  $i'$  bands. The image at 155 days is devoid of afterglow and SN contribution, and the host galaxy is faintly seen in the  $i'$  band. The images have been smoothed for display purposes.

$E(B - V) = 1.80$  mag (Fulton et al. 2023; Williams et al. 2023). Given these uncertainties, we consider the implications of differing host extinction levels throughout this work.

Finally we correct for underlying host galaxy light in our analysis, derived by Levan et al. (2023) through GALFITM modeling of late-time Hubble Space Telescope (HST) observations. We use their measurements of  $F625W = 24.88 \pm 0.08$  mag and  $F775W = 23.80 \pm 0.14$  mag, which approximately correspond to the  $r'$  and  $i'$  bands. Previous analyses (Fulton et al. 2023; Kann et al. 2023; Shrestha et al. 2023) did not incorporate the host contribution explicitly in their analysis (though Pan-STARRS and DECam photometry in Fulton et al. 2023, and DECam photometry in Shrestha et al. 2023 are subjected to template subtraction, which negates the host contribution to a degree).

### 3.2. Optical Afterglow Modeling

Assuming the optical afterglow is powered by synchrotron emission from the forward shock (Mészáros & Rees 1997), we fit the early-time light curve with power-law models ( $f_\nu \propto t^{-\alpha}$ ) to attempt to isolate the contribution from the SN. Prior to  $T_0 + 1$  day, the optical data display a shallow initial slope with  $\alpha = 0.88 \pm 0.05$  (Kann et al. 2023; O'Connor et al. 2023). Beyond this time there is a clear steepening in the decay, and a single power law does not provide a good fit to all optical data (D'Avanzo et al. 2022).

Since a SN will contribute negligibly (compared to the bright afterglow here) in the first days postexplosion, we perform a

power-law fit of all  $g'$ ,  $r'$ ,  $i'$ , and  $z'$  data between 1 and 6 days postexplosion. We find a best-fit decay index of  $\alpha = 1.434 \pm 0.004$ . As found by other authors, this index is appreciably shallower than the X-ray decay found at this time (Laskar et al. 2023; O'Connor et al. 2023; Williams et al. 2023). Figure 2 shows the best-fit power law derived, along with the addition of the host galaxy emission to that power law.

The late-time behavior shows possible deviations from this power law, even after the host galaxy emission is considered. Though it is possible that central-engine activity can cause rebrightening of the optical afterglow in excess of what is expected from a power-law decay, this usually occurs directly after the prompt emission in the early-time evolution of the GRB (Kann et al. 2007; Oates et al. 2009). Because the brightening occurs weeks after the initial prompt emission (see Figure 1), we determine that there is the possibility that an associated SN is contributing excess flux to the optical emission, and further investigate this in Section 3.3.

### 3.3. Model Selection

In order to evaluate the statistical significance of the excess late-time emission, we perform a Bayesian model selection using the PYMULTINEST package (Feroz et al. 2009; Buchner et al. 2014). We consider two empirical models—one where the optical emission is explained as the sum of the afterglow (i.e., synchrotron radiation) and a (constant) host galaxy emission, and one where an additional SN component is added. For each model, we calculate the Bayesian evidence,

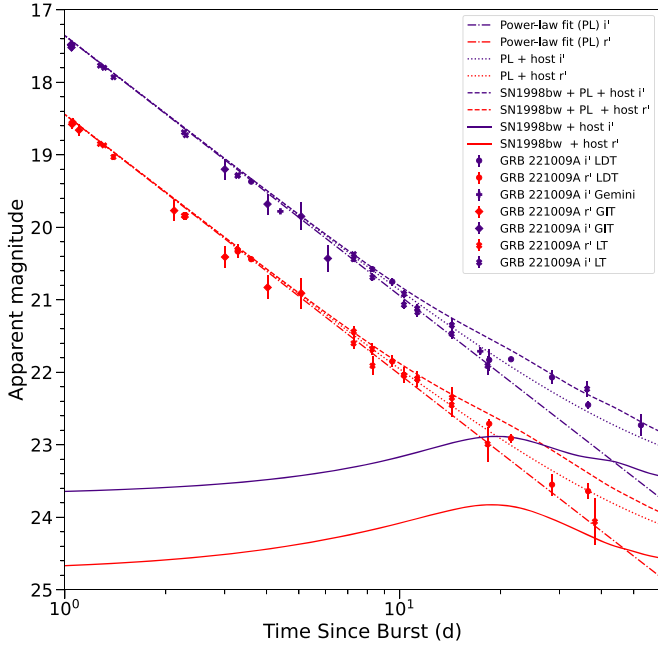


**Figure 2.** Observed  $r'$ - and  $i'$ -band photometry of GRB 221009A after  $T_0 + 1$  day, along with the best-fit optical afterglow model corresponding to a power-law decay index of  $\alpha = 1.434$ , with the addition of the host galaxy emission. The light curves for a SN 1998bw-like source in the  $r'$  and  $i'$  band, redshifted to  $z = 0.151$  and reddened according to the Galactic and host galaxy extinction of GRB 221009A, are also shown.

and use it to calculate the Bayes factor to see which is statistically preferred (Trotta 2008). We limit the analysis to the  $r'$  and  $i'$  bands, as the large Galactic extinction makes  $g'$  band uninformative, and  $z'$  band SN templates are less available due to a lack of spectral coverage in that wavelength range.

For the afterglow+host model, we assume a single power-law decay in both bands at times after  $T_0 + 1$  day. While the index is fixed to be identical in both the  $r'$  and  $i'$  bands, we do not require its value be equal to that derived from 1 to 6 days postexplosion (Section 3.2); rather, we allow the index to vary to provide the best fit to the entire data set. The host galaxy emission is incorporated as a free parameter in the fit, using a Gaussian prior with the mean and standard deviation measured by HST (Levan et al. 2023).

For the SN model, an additional component is added to the afterglow+host model to mimic SN behavior. We take the light curve of SN 1998bw (Clocchiatti et al. 2011), and (de)dden and  $K$ -correct it to match the relevant properties of GRB 221009A, using SNCOSMO (Barbary et al. 2016). Specifically we adopt  $E(B - V)_{\text{MW}} = 1.30$  mag (Schlafly & Finkbeiner 2011),  $E(B - V)_{\text{host}} = 0.3$  mag, which is the most conservative value found in Williams et al. (2023), and apply the Milky Way extinction law from Cardelli et al. (1989) with  $R_V = 3.1$ . The resulting  $r'$  and  $i'$ -band light curves for a SN 1998bw-like source at  $z = 0.151$  [and behind an extinction of  $E(B - V)_{\text{MW}} = 1.30$  mag and  $E(B - V)_{\text{host}} = 0.3$  mag] are shown in Figure 2.

The final SN model used in the model selection has two free parameters: a flux-stretching factor  $k_{\text{SN } 1998\text{bw}}$  and a time-stretching factor  $s_{\text{SN } 1998\text{bw}}$  (e.g., Klose et al. 2019). Both of these parameters have priors drawn from a bivariate normal distribution fit to values derived for previous GRB-SNe (Cano et al. 2017). We also allow the afterglow power-law decay

index ( $\alpha$ ) to be free with uniform priors, the flux constants of proportionality ( $a_{\text{AG}}$ ) to be free with uniform priors in log space, and add the host galaxy emission in both bands utilizing the same Gaussian priors. Therefore, the full SN model is:

$$f_{\nu}(t_{\text{obs}}) = k_{\text{SN}}(f_{\nu}^{\text{SN } 1998\text{bw}}(t_{\text{obs}}/s_{\text{SN } 1998\text{bw}})) + a_{\text{AG}}(t_{\text{obs}})^{-\alpha} + f_{\nu}^{\text{host}}, \quad (1)$$

where  $f_{\nu}^{\text{SN } 1998\text{bw}}(t_{\text{obs}})$  is the flux seen of the SN at a time in the observer frame,  $t_{\text{obs}}$  is the time in the observer frame, and  $f_{\nu}^{\text{host}}$  is the flux contribution from the host galaxy.

Initially, we fit the two models concurrently to the  $r'$  and  $i'$  bands, while assuming the errors are the nominal values reported in Table 1 and Laskar et al. (2023) for the LT photometry. We calculate the Bayes factor ( $K_{\text{Bayes}}$ ) between the two models to determine the likelihood that an SN is contributing excess flux to the optical afterglow in addition to the host galaxy emission, and find  $K_{\text{Bayes}} = 10^{4.0}$ , which indicates that the SN model is strongly favored. However, when we calculate the  $\chi^2$  statistic for each of the models, we find that  $\chi^2_{\text{PL+host}} = 120.83$  for  $62^\circ$  of freedom and  $\chi^2_{\text{PL+host+SN}} = 112.62$  for  $60^\circ$  of freedom. Though the  $\Delta\chi^2 = 8.21$  for two additional degrees of freedom is also indicative of a preference for the SN model, the  $\chi^2$  statistics themselves indicate that neither model adequately fits the data. This is likely because in the initial fitting, we did not account for systematic uncertainties that arise from combining data from multiple telescopes in the full photometric data set, or  $S$ -corrections (Stritzinger et al. 2002).

Therefore, we modify the fitting procedure to optimize the likelihood function numerically, where we assume that the reported errors underestimate the true uncertainty. To account for this, we include an error-stretching factor ( $\beta$ ) in the fitting procedure to represent the  $S$ -correction effect, and recalculate  $K_{\text{Bayes}}$ . The log-likelihood function we minimize, with the addition of the error-stretching factor, is:

$$\ln p(y | m, s_n) = -\frac{1}{2} \sum_n \frac{(y_n - m_n)^2}{s_n^2} + \ln(2\pi s_n^2), \quad (2)$$

where  $y_n$  are the observed data,  $m_n$  are the modeled data, and  $s_n^2$  are:

$$s_n^2 = \sigma_n^2 + \beta^2(m_n^2), \quad (3)$$

where  $\sigma_n$  are the nominal errors to the observed data.

The new Bayes factor we find is  $K_{\text{Bayes}} = 10^{1.2}$ , which indicates the SN model is moderately, but not conclusively, preferred. We report the median parameters with their  $1\sigma$  errors, along with the best-fit parameters which minimize the log-likelihood function in Table 2. The best-fit models are shown in Figure 3, along with their associated  $\chi$  values. According to the model selection analysis, the optimal error-stretching factor increases the error bars by  $\sim 3\%$  with respect to the model value at the observed time, for both the afterglow+host and SN model. We also calculated the Bayesian evidence for the two models, while incorporating independent error-stretching factors ( $\beta_i$ ) for each telescope rather than a single factor across all data sets. We did so to investigate if the way we account for systematic uncertainties plays a role in biasing the model preferences. We still find similar results, as the SN model is favored by a Bayes factor of  $K_{\text{Bayes}} = 10^{0.7}$ .

**Table 2**  
Bayesian Model Selection Fitting Parameters for the Afterglow+host and the Afterglow+Host+SN Models

	$a_{r'}$ ( $\mu\text{Jy}$ )	$a_{i'}$ $a_{i', \text{AG}}$	$\alpha$	$f_{\nu, r'}^{\text{host}}$ ( $\mu\text{Jy}$ )	$f_{\nu, i'}^{\text{host}}$ ( $\mu\text{Jy}$ )	$k_{\text{SN } 1998\text{bw}}$	$s_{\text{SN } 1998\text{bw}}$	$\ln(\beta)$
Afterglow+Host (Best fit)	146	388	1.43	0.44	1.64	...	...	-3.37
Afterglow+Host (Median $\pm 1\sigma$ )	$144 \pm 2$	$384^{+5}_6$	$1.42 \pm 0.01$	$0.41 \pm 0.03$	$1.33 \pm 0.11$	...	...	$-3.30 \pm 0.21$
Afterglow+Host+SN (Best fit)	147	394	1.46	0.35	1.17	0.39	0.69	-3.51
Afterglow+Host+SN (Median $\pm 1\sigma$ )	$146 \pm 2$	$395^{+5}_6$	$1.47 \pm 0.01$	$0.39 \pm 0.03$	$1.12^{+0.11}_{-0.12}$	$0.43 \pm 0.10$	$0.63 \pm 0.09$	$-3.50^{+0.23}_{-0.24}$

Next, we analyze the LDT and LT photometry separately using their nominal error bars, to identify if the combination of photometry from different telescopes plays a role in biasing the model preferences. We do not fit the Gemini-South and GIT photometry separately, as there are only two Gemini-South photometry points, and the GIT photometry are all at early times where any SN excess contributing to the afterglow would be negligible. We find that the afterglow+host model is favored with a Bayes factor of  $K_{\text{Bayes}} = 10^{0.9}$  for the LDT photometry, while the two models are indistinguishable for the LT photometry. Figure 2 shows that the majority of the LDT photometry is at late times, where excess flux from a SN would be identifiable. This, in addition to only five and six photometry points being available respectively in the  $r'$  and  $i'$  bands leads to the model selection converging toward a shallow power-law decay slope in its fitting procedure, in order to fit for the excess flux. The best-fit power-law decay index is  $\alpha = 1.36$  (median  $\pm 1\sigma = 1.36 \pm 0.02$ ), which is shallower than what is derived from the early-time optical photometry fitting in Section 3.2. Therefore, although the afterglow+host model is preferred for the LDT data, the lack of early-time data biases the fit toward a power-law decay index that is shallower than expected in order to fit for the excess flux.

On the other hand, the majority of LT data are at early times and at a significantly higher cadence than the LDT photometry. The best-fit power-law decay index for the afterglow+host model is  $\alpha = 1.46$  (median  $\pm 1\sigma = 1.45 \pm 0.01$ ), which is consistent with the power-law decay index derived in Section 3.2. The two models are indistinguishable due to a few photometry points that do show excess emission at later times, for which the afterglow model cannot account. Therefore, it is necessary to incorporate a combination of data sets in the modeling, in order to have optimal temporal coverage such that a sufficient amount of photometry points at both early and late times is accounted for in the fitting. After accounting for  $S$ -corrections modeled through our error-stretching factor, it is clear that the most accurate physical description of the light curve comes from incorporating the entire data set, which we find favors the SN model moderately.

As a final sanity check, we perform a similar analysis using the observed light curve of SN 2013dx associated with GRB 130702A (D'Elia et al. 2015; Toy et al. 2016) with the extinction values described above, again optimizing the likelihood function and allowing for an error-stretching factor. Due to the similar redshift ( $z = 0.145$ ) to GRB 221009A, this avoids the requirement of calculating  $K$ -corrections (Fulton et al. 2023; Shrestha et al. 2023). In this case we find a comparable Bayes factor to the analysis using SN 1998bw:  $K_{\text{Bayes}} = 10^{0.7}$ , preferring the SN model. Thus we infer that the SN model preference is relatively insensitive to the details of the template SN used. We also emphasize that the detailed value of the host extinction adopted has little impact on the

model selection. Since the SN flux is scaled by the free parameter  $k_{\text{SN}}$ , increasing or decreasing the host extinction is largely offset in the modeling by a corresponding change in  $k_{\text{SN}}$ .

Our preference for the SN model agrees with Fulton et al. (2023), as they find significant evidence of excess emission in the optical afterglow that is well modeled by an additional SN component. However, they did not account for host galaxy emission explicitly in their analysis, and Figure 2 shows that the host galaxy makes nonnegligible contributions to the optical afterglow at late times. This is likely why they were able to find significant evidence of excess emission, while our preference for the SN model is moderate. Shrestha et al. (2023) and Levan et al. (2023) report no evidence for *bright* SN emission, while Kann et al. (2023) does not find any strong evidence for or against SN emission. None of them rule out the possibility of a faint associated SN, and one of the conclusions of Levan et al. (2023) is that an associated SN to GRB 221009A must be either substantially ( $\sim 10\%$ – $40\%$ ) fainter or bluer than SN 1998bw. Our findings point toward the former being true, as the best-fit flux-scaling factor for SN 2022xiw with respect to SN 1998bw is  $k_{\text{SN } 1998\text{bw}} = 0.39$ , with an upper limit at the 99% confidence interval of  $k_{\text{SN } 1998\text{bw}} < 0.67$ .

## 4. SN Parameter Estimation

### 4.1. Nickel Mass Estimates

After demonstrating a preference for models including a SN component, we derive flux measurements for SN 2022xiw by subtracting the the best-fit optical afterglow model (see Section 3.2) from the observed  $r'$ - and  $i'$ -band photometry. We only use photometry starting from  $T_0 + 7$  days, and convert negative flux values after the subtractions to  $3\sigma$  upper limits. The resulting SN light curve is shown in Figure 4. The SN photometry shown in the Figure is not host subtracted, because we allow the host galaxy emission to vary as a free parameter within the Gaussian priors corresponding to the values from Levan et al. (2023) when extracting physical parameters from the light curve.

The decay of  $^{56}\text{Ni}$  to  $^{56}\text{Co}$  and to  $^{56}\text{Fe}$  releases the energy that powers the optical light curve of Type I SNe, so the  $^{56}\text{Ni}$  mass is a key physical parameter that can provide insight into the properties of the explosion and progenitor (Arnett 1982; hereafter A82). Therefore, we fit semianalytic light-curve models from A82 to the observed  $r'$ - and  $i'$ -band photometry after day 7 to constrain the  $^{56}\text{Ni}$  mass. Equation (36) in A82 provides an analytic expression for the bolometric luminosity of Type I SNe, assuming full  $\gamma$ -ray trapping of the ejecta along with further radioactive inputs (Valenti et al. 2008). We use the infrastructure from the Hybrid Analytic Flux FittEr for Transients (HAFFET; Yang & Sollerman 2023) to perform

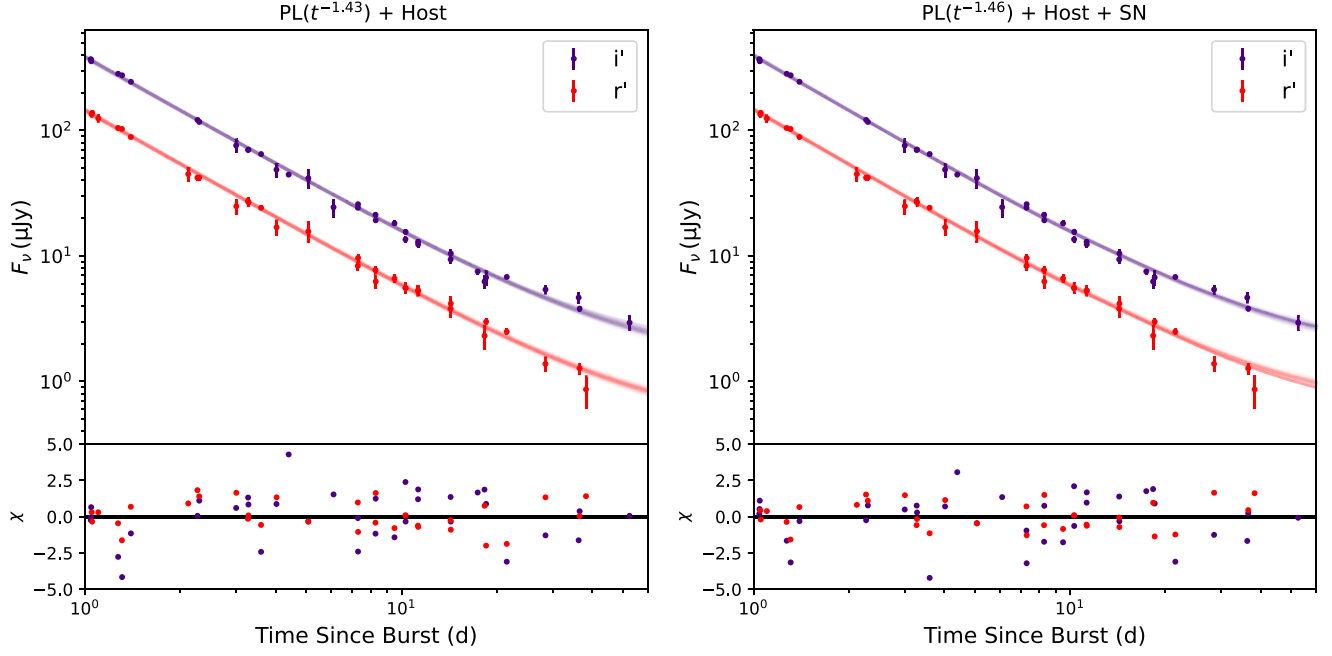


**Figure 3.** Left panel: the best-fit afterglow+host model, along with its a posteriori possible models and  $\chi$  values. Right panel: the best-fit SN model, along with its a posteriori models and  $\chi$  values. The SN model is moderately but not conclusively favored, with a Bayes factor  $K_{\text{Bayes}} = 10^{1.2}$ , and the best-fit parameters for each model are shown in Table 2.

the fits, where the two free parameters are the nickel mass ( $M_{\text{Ni}}$ ) and the photon diffusion timescale ( $\tau_{\text{m}}$ ).

Given a bolometric light curve from the model, it is necessary to extract the associated  $r'$ - and  $i'$ -band light curves to compare to the observed photometry. It is possible to derive light curves in individual bands from a bolometric magnitude light curve using bolometric correction (BC) coefficients:

$$\text{BC}_x = M_{\text{bol}} - M_x, \quad (4)$$

where  $x$  is the relevant filter.

For stripped-envelope SNe, Lyman et al. (2014) derive a  $g$ -band BC coefficient of:

$$\text{BC}_g = 0.054 - 0.195 \times (g - r) - 0.719 \times (g - r)^2. \quad (5)$$

Here we assume that the color evolution of SN 2022xiw is identical to that of SN 1998bw. We use the BC coefficient, along with the color evolution of SN 1998bw, to generate  $r'$ - and  $i'$ -band light curves to fit to the SN photometry. First, we convert the  $BVRI$  photometry of SN 1998bw from Clocchiatti et al. (2011) to Sloan Digital Sky Survey (SDSS) filters using conversions from Jester et al. (2005). At the time of each observation, we compute  $\text{BC}_g$ , along with the  $g - r$  and  $g - i$  colors. Given a bolometric absolute magnitude light curve from A82, we derive a  $g$ -band absolute magnitude light curve from  $\text{BC}_g$ . We then compute the associated  $r$ - and  $i$ -band light curves from the  $g - r$  and  $g - i$  colors derived above. Finally we apply the distance modulus, host galaxy emission, and extinction corrections described below, along with conversions from  $r$  and  $i$  band to  $r'$  and  $i'$  band,<sup>28</sup> to produce observed  $r'$ - and  $i'$ -band light curves for comparison with the data. Best-fit models with associated uncertainties are generated using Markov Chain Monte Carlo (MCMC) techniques.

Given the large uncertainty in the host extinction (Section 3.1), we perform the fitting under three different assumptions: (1)  $E(B - V)_{\text{host}}$  allowed to vary freely between 0.3 and 0.5 mag; (2)  $E(B - V)_{\text{host}}$  fixed to a value of 0.3 mag; and, (3)  $E(B - V)_{\text{host}}$  fixed to a value of 0. For all three scenarios we allow  $M_{\text{Ni}}$ ,  $\tau_{\text{m}}$ , and  $E(B - V)_{\text{MW}}$  to vary as additional free parameters. We allow  $E(B - V)_{\text{MW}}$  to vary due to the high uncertainty in the Galactic extinction at the location of GRB 221009A, and adopt uniform priors corresponding to the minimum and maximum values from Schlafly & Finkbeiner (2011). Additionally, we allow the host galaxy emission in the  $r'$  and  $i'$  bands to vary as free parameters, with Gaussian priors corresponding to the values presented in Levan et al. (2023). We adopt uniform priors for  $M_{\text{Ni}}$  and  $\tau_{\text{m}}$  based on values from previous Type Ic-BL SN studies (Corsi et al. 2016, 2022; Taddia et al. 2019).

We note that there are varying interpretations of the intrinsic extinction and hydrogen column density of the host that are model dependent on the spectral shape of the afterglow (e.g.,  $E(B - V)_{\text{host}} < 0.1$  mag, O'Connor et al. 2023;  $N_{\text{H}} \approx 4 \times 10^{21} \text{ cm}^{-2}$ , Tiengo et al. 2023). However, we believe that the most likely physically plausible situation is the first where  $E(B - V)_{\text{host}}$  is allowed to vary freely between 0.3 and 0.5 mag, due to the possibility of a significant amount of intrinsic hydrogen column density in the host that may be up to  $N_{\text{H}} \approx 1.29 \times 10^{22} \text{ cm}^{-2}$  (Williams et al. 2023). We present the best-fit model from this scenario and 100 random samples from the posterior distribution in Figure 4, along with the associated corner plots for each parameter.

The best-fit values derived in all three scenarios are displayed in Table 3, and we find  $M_{\text{Ni}} = 0.05\text{--}0.25 M_{\odot}$ , depending on the scenario. Because the SN flux is only marginally detectable with respect to the afterglow and host galaxy emission, these best-fit values should be taken with a grain of salt. However, we can more robustly determine an upper limit, and find that at the 99% confidence level,  $M_{\text{Ni}} < 0.36 M_{\odot}$ . The  $M_{\text{Ni}}$  we find is systematically lower than

<sup>28</sup> [https://classic.sdss.org/dr5/algorithms/jeg\\_photometric\\_eq\\_dr1.html##usno2SDSS](https://classic.sdss.org/dr5/algorithms/jeg_photometric_eq_dr1.html##usno2SDSS)

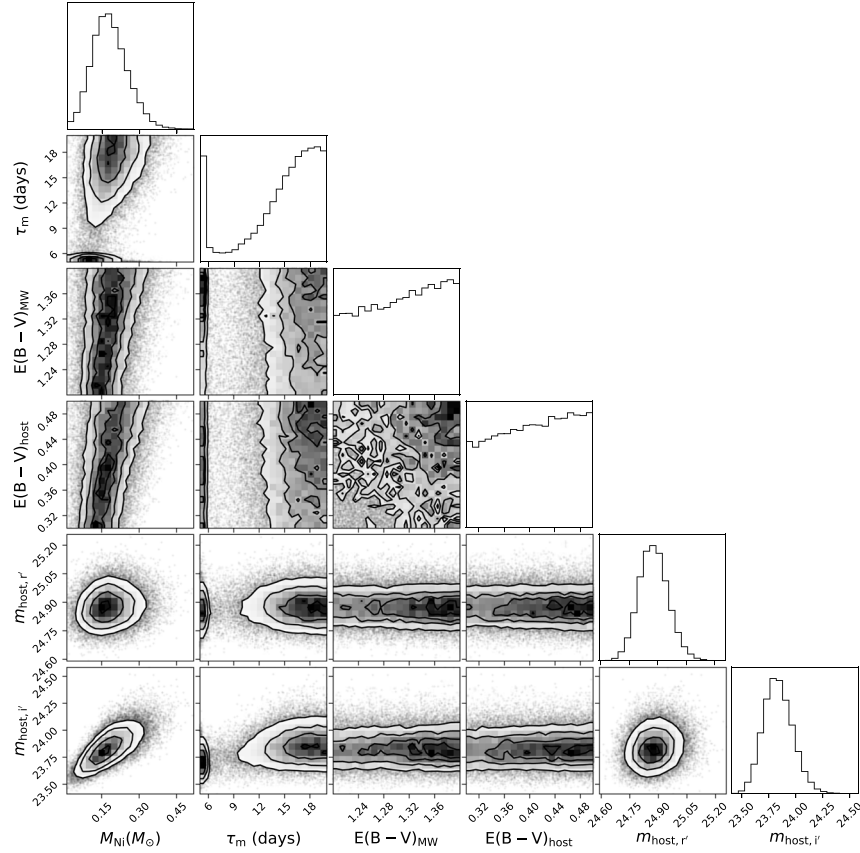
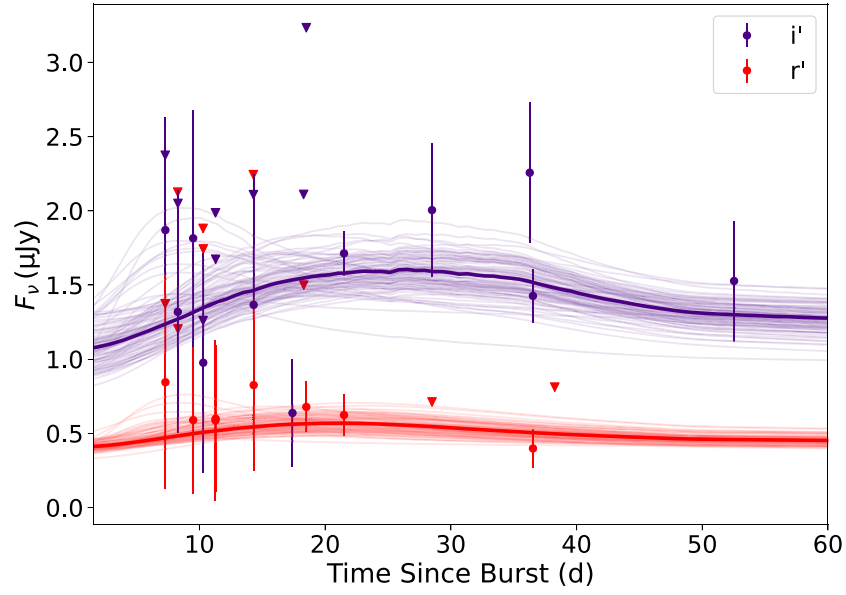


**Figure 4.** Top panel: best-fit  $r'$ - and  $i'$ -band light curves in flux space extrapolated from the best-fit bolometric light curve constructed from the **A82** model (details in Section 4), assuming the host galaxy extinction is a free parameter between  $E(B - V)_{\text{host}} = 0.3\text{--}0.5$  mag. The best-fit values are  $M_{\text{Ni}} = 0.18^{+0.07}_{-0.06} M_{\odot}$ ,  $\tau_m = 15.98^{+2.77}_{-5.36}$  days,  $E(B - V)_{\text{MW}} = 1.31^{+0.06}_{-0.07}$  mag,  $E(B - V)_{\text{host}} = 0.41^{+0.06}_{-0.07}$  mag,  $m_{\text{host}, r'} = 24.88^{+0.08}_{-0.07}$  mag, and  $m_{\text{host}, i'} = 23.83^{+0.14}_{-0.12}$  mag. 100 random posteriori possible models from the MCMC fitting samples are plotted, along with the best fits in bold. Bottom panel: corner plots associated with the MCMC fits of the **A82** model, corresponding to the top panel. A total of 33,250 samples were generated in the posteriors.

that of SN 1998bw ( $M_{\text{Ni}} = 0.3\text{--}0.9 M_{\odot}$ ; Sollerman et al. 2000), which agrees with the results from Section 3.3, that SN 2022xiw must be substantially fainter than SN 1998bw.

Finally, we note that if we repeat the analysis under the same assumptions as Fulton et al. (2023), who do not explicitly account for host galaxy emission, and assume an additional 0.8 mag of

extinction in the optical when compared to the nominal galactic extinction from Schlafly & Finkbeiner (2011), we find  $M_{\text{Ni}} = 0.59 \pm 0.04 M_{\odot}$ . This  $M_{\text{Ni}}$  is lower, but marginally consistent with their value of  $M_{\text{Ni}} = 1.0^{+0.6}_{-0.4} M_{\odot}$ . The lower  $M_{\text{Ni}}$  in comparison to their work is expected, due to their use of a steeper optical afterglow power-law decay slope ( $f_{\nu} \propto t^{-1.556 \pm 0.002}$ ,



**Table 3**  
Best-fit Physical Parameters and Their Statistical  $1\sigma$  Errors Corresponding to the Three Different Host Extinction Scenarios Presented in Section 4.1

	$M_{\text{Ni}}$ ( $M_{\odot}$ )	$\tau_{\text{m}}$ (days)	$E(B - V)_{\text{MW}}$ (mag)	$E(B - V)_{\text{host}}$ (mag)	$M_{\text{ej}}$ ( $M_{\odot}$ )	$E_{\text{KE}}$ (erg)	$m_{\text{host}}, r'$ (mag)	$m_{\text{host}}, i'$ (mag)
$E(B - V)_{\text{host}} = 0.3\text{--}0.5$ mag	$0.18^{+0.07}_{-0.06}$	$15.98^{+2.77}_{-5.36}$	$1.31^{+0.06}_{-0.07}$	$0.41^{+0.06}_{-0.07}$	$7.93^{+2.99}_{-4.43}$	$3.71^{+1.40}_{-2.07} \times 10^{52}$	$24.88^{+0.08}_{-0.07}$	$23.83^{+0.14}_{-0.12}$
$E(B - V)_{\text{host}} = 0.3$ mag	$0.14^{+0.05}_{-0.04}$	$16.56^{+2.35}_{-3.24}$	$1.31^{+0.06}_{-0.07}$	0.3	$8.53^{+2.59}_{-3.01}$	$3.99^{+1.21}_{-1.41} \times 10^{52}$	$24.88^{+0.08}_{-0.07}$	$23.84^{+0.13}_{-0.12}$
$E(B - V)_{\text{host}} = 0$ mag	$0.07 \pm 0.02$	$16.26^{+2.52}_{-3.34}$	$1.31^{+0.06}_{-0.07}$	0	$8.22^{+2.74}_{-3.03}$	$3.84^{+1.28}_{-1.42} \times 10^{52}$	$24.89^{+0.08}_{-0.07}$	$23.82^{+0.13}_{-0.11}$

see Section 3.1), which in turn leads to more luminous SN emission, and a higher  $M_{\text{Ni}}$ .

#### 4.2. Additional Explosion Properties

Given the photon diffusion timescale  $\tau_{\text{m}}$ , it is possible to derive the total ejecta mass ( $M_{\text{ej}}$ ) of a SN, through Equation A1 of Valenti et al. (2008):

$$\tau_{\text{m}}^2 = \frac{2\kappa_{\text{opt}}M_{\text{ej}}}{\beta c v_{\text{sc}}}, \quad (6)$$

where  $\kappa_{\text{opt}} = 0.07 \text{ cm}^{-2} \text{ g}^{-1}$  is a constant, average opacity that is able to produce consistent results with hydrodynamical light-curve modeling of stripped-envelope SNe (Taddia et al. 2018),  $\beta = 13.8$  is a constant,  $c$  is the speed of light, and  $v_{\text{sc}}$  is a scale velocity, which is set observationally to the photospheric velocity  $v_{\text{ph}}$ , which is roughly related to the line velocity at the peak epoch.

Given that we assumed the color and spectral evolution of SN 2022xiw were identical to that of SN 1998bw, we also assume it has a comparable photospheric velocity:  $v_{\text{ph}} = 28,000 \text{ km s}^{-1}$  (Iwamoto et al. 1998). We note that SN 1998bw's photospheric velocity is high with respect to the population of GRB-SNe in the literature, which possess an average of  $v_{\text{ph}} = 20,200 \text{ km s}^{-1}$ , with a dispersion  $\sigma = 8500 \text{ km s}^{-1}$  (Cano et al. 2017). However, a spectrum taken of the optical afterglow at  $T_0 + 8$  days reported the possible existence of broad features with velocities slightly larger than SN 1998bw (de Ugarte Postigo et al. 2022b). Therefore, our assumption of SN 2022xiw's peak photospheric velocity is valid, and may possibly underrepresent the true photospheric velocity. We report the derived values in Table 3, and find  $M_{\text{ej}} = 3.5\text{--}11.1 M_{\odot}$ .

Given  $M_{\text{ej}}$  and  $v_{\text{sc}}$ , it is possible to derive the kinetic energy  $E_{\text{KE}}$  of the explosion, assuming that it is a constant density sphere undergoing homologous expansion (Lyman et al. 2016):

$$v_{\text{sc}}^2 \equiv v_{\text{ph}}^2 = \frac{5}{3} \frac{2E_{\text{K}}}{M_{\text{ej}}}. \quad (7)$$

The derived values are again reported in Table 3, and we find  $E_{\text{KE}} = (1.6\text{--}5.2) \times 10^{52} \text{ erg}$ . These values are consistent with the values Fulton et al. (2023) derive, who find  $M_{\text{ej}} = 7.1^{+2.4}_{-1.7} M_{\odot}$  and  $E_{\text{KE}} = (2.7\text{--}6.3) \times 10^{52} \text{ erg}$ . We note that both  $M_{\text{ej}}$  and  $E_{\text{K}}$  largely depend on the photon diffusion timescale, and the corner plots in Figure 4 show that  $\tau_{\text{m}}$  is close to hitting the bounds of the priors. This is unsurprising given the nature of the data set, and the faintness of the SN with respect to the afterglow and host galaxy emission. Therefore, both the  $M_{\text{ej}}$  and  $E_{\text{KE}}$  we derive should also be considered as estimates, and we are unable to derive robust upper limits in this case due to the nature of the posterior of  $\tau_{\text{m}}$ .

We note that throughout this analysis, systematic uncertainties likely arise from the assumptions made with the color and spectral evolution of SN 2022xiw being identical to that of SN 1998bw, as well as assuming that the explosion is undergoing homologous expansion, as the presence of a relativistic jet likely impacts the spherical symmetry of the explosion. An asymmetric explosion would likely impact  $\kappa_{\text{opt}}$  and the assumptions made in Equation (6) from Taddia et al. (2019). However, despite these caveats, the statistical uncertainties we find are large and likely dominate over any of these systematic uncertainties.

### 5. Comparison to other GRB-SNe

Based on our previous modeling, we attempt to contextualize SN 2022xiw with respect to the overall GRB-SN population. The range of  $M_{\text{Ni}}$  found for previous GRB-SNe, derived under the same assumption that the luminosity is powered by the radioactive decay of  $^{56}\text{Ni}$ , has an average value of  $M_{\text{Ni}} = 0.37 M_{\odot}$  with a dispersion  $\sigma = 0.20 M_{\odot}$  (Cano et al. 2017). The  $M_{\text{Ni}}$  we derive for the scenarios where we take into account host galaxy extinction ( $M_{\text{Ni}} = 0.10\text{--}0.25 M_{\odot}$ ) are within this range, while the  $M_{\text{Ni}}$  we derive for the scenario with zero host galaxy extinction is outside of this range. The upper limit for the  $M_{\text{Ni}}$  we derive ( $<0.36 M_{\odot}$ ) shows that despite GRB 221009A's highly energetic nature, its associated SN does not possess an exceptional  $M_{\text{Ni}}$  in comparison with the overall GRB-SN population—in fact, its  $M_{\text{Ni}}$  is likely lower with respect to the average. For the ejecta mass and kinetic energy, the average values inferred for previous GRB-SNe are  $M_{\text{ej}} = 6 M_{\odot}$  with a dispersion  $\sigma = 4 M_{\odot}$  and  $E_{\text{KE}} = 2.5 \times 10^{52} \text{ erg}$ , with a dispersion  $\sigma = 1.8 \times 10^{52} \text{ erg}$  (Cano et al. 2017). Despite the caveat mentioned in Section 4.2 with the values we derive, both the ejecta masses and kinetic energies for all scenarios are well within these values.

Through these comparisons, we see that SN 2022xiw possesses explosion properties that are overall broadly consistent with the GRB-SN population. This is despite its highly energetic relativistic ejecta, as it possesses an isotropic-equivalent peak  $\gamma$ -ray luminosity of  $L_{\gamma, \text{iso}} = 2.1 \times 10^{54} \text{ erg s}^{-1}$  (Frederiks et al. 2023), making it the most luminous GRB-SN ever detected (Cano et al. 2017; Burns et al. 2023). Figure 3 in Hjorth (2013) suggests that a relationship may exist between the energy release of GRBs and their associated SN brightness. In his Figure 3, he plots the  $L_{\gamma, \text{iso}}$  of GRBs against the peak absolute magnitude in V band ( $M_{\text{V}}$ ) of their associated SNe, and make the distinction between low-luminosity GRBs ( $L_{\gamma, \text{iso}} < 10^{48.5} \text{ erg s}^{-1}$ ), and high-energy jet GRBs ( $L_{\gamma, \text{iso}} > 10^{49.5} \text{ erg s}^{-1}$ ). He reports a possible direct relationship between  $L_{\gamma, \text{iso}}$  and  $M_{\text{V}}$  in low-luminosity GRBs, which turns over into a possible inverse relationship in the high-energy jet GRB region of the parameter space.

In Figure 5, we recreate the results from Hjorth (2013) to test for these correlations, with a larger data set and a few

**Table 4**

Optical Photometry and  $1\sigma$  Errors of GRB 221009A, Including Contributions From its Afterglow, Host Galaxy, and Associated SN 2022xiw, From Publicly Available GCNs

$t_{\text{obs}} - T_0$ (days)	Filter	AB mag	Uncertainty
0.128349	<i>g</i>	17.66	0.07
0.211	<i>g</i>	18.22	0.33
1.134	<i>g</i>	20.43	0.2
1.152193	<i>g</i>	20.13	0.08
1.165	<i>g</i>	20.53	0.11
2.166539	<i>g</i>	21.15	0.21
1.02802141	<i>g</i>	20.037	0.205
1.03149415	<i>g</i>	20.248	0.234
1.12791174	<i>g</i>	20.228	0.339
1.13782442	<i>g</i>	20.299	0.363
1.1412292	<i>g</i>	20.634	0.469
1.27027935	<i>g</i>	20.33	0.06
1.39404935	<i>g</i>	20.41	0.12
2.29360935	<i>g</i>	21.05	0.12
3.28066935	<i>g</i>	21.61	0.19
6.09	<i>g</i>	22.61	0.12
11.55024	<i>g</i>	23.7	0.2
0.131049	<i>r</i>	16.16	0.07
0.211	<i>r</i>	16.76	0.08
0.43625	<i>r</i>	17.36	0.12
1.136	<i>r</i>	18.57	0.05
1.159669	<i>r</i>	18.65	0.02
1.168	<i>r</i>	18.64	0.03
1.172	<i>r</i>	18.43	0.11
1.2568	<i>r</i>	18.74	0.12
1.301	<i>r</i>	18.96	0.1
1.314699	<i>r</i>	18.81	0.05
2.138926	<i>r</i>	19.53	0.04
2.306539	<i>r</i>	19.67	0.11
3.156539	<i>r</i>	20.03	0.06
3.176539	<i>r</i>	19.97	0.08
3.206539	<i>r</i>	20.07	0.19
3.226539	<i>r</i>	20.32	0.17
3.2459	<i>r</i>	20.23	0.09
3.266539	<i>r</i>	20.17	0.12
3.296539	<i>r</i>	20.26	0.16
3.316539	<i>r</i>	20.24	0.19
4.146539	<i>r</i>	20.53	0.09
4.176539	<i>r</i>	20.63	0.09
4.196539	<i>r</i>	20.71	0.15
4.216539	<i>r</i>	20.54	0.1
4.236539	<i>r</i>	20.55	0.12
4.266539	<i>r</i>	20.74	0.16
4.286539	<i>r</i>	20.9	0.23
4.306539	<i>r</i>	20.86	0.27
4.674099	<i>r</i>	20.92	0.05
5.7	<i>r</i>	21.13	0.06
0.214	<i>i</i>	15.58	0.03
1.154	<i>i</i>	17.56	0.05
1.167041	<i>i</i>	17.52	0.01
1.17	<i>i</i>	17.58	0.01
1.322576	<i>i</i>	17.69	0.02
1.48	<i>i</i>	17.92	0.11
2.14674	<i>i</i>	18.4	0.02
2.316539	<i>i</i>	18.49	0.04
3.146539	<i>i</i>	18.82	0.03
3.176539	<i>i</i>	19.02	0.07
3.196539	<i>i</i>	19.09	0.1
3.216539	<i>i</i>	18.95	0.07
3.236539	<i>i</i>	18.93	0.04
3.2459	<i>i</i>	18.91	0.11
3.266539	<i>i</i>	18.93	0.04
3.286539	<i>i</i>	18.92	0.04

**Table 4**

(Continued)

$t_{\text{obs}} - T_0$ (days)	Filter	AB mag	Uncertainty
4.156539	<i>i</i>	19.51	0.06
4.176539	<i>i</i>	19.41	0.05
4.206539	<i>i</i>	19.52	0.05
4.226539	<i>i</i>	19.44	0.04
4.246539	<i>i</i>	19.45	0.05
4.266539	<i>i</i>	19.43	0.05
4.296539	<i>i</i>	19.48	0.06
4.316539	<i>i</i>	19.5	0.07
4.45	<i>i</i>	19.89	0.05
4.671579	<i>i</i>	19.88	0.02
5.7	<i>i</i>	20.01	0.05
6.07	<i>i</i>	20.01	0.04
0.216667	<i>z</i>	14.89	0.03
1.166	<i>z</i>	16.93	0.05
1.171	<i>z</i>	16.87	0.05
1.174389	<i>z</i>	16.81	0.01
1.330626	<i>z</i>	16.99	0.01
1.48	<i>z</i>	16.92	0.11
2.154231	<i>z</i>	17.69	0.02
2.326539	<i>z</i>	17.72	0.03
3.166539	<i>z</i>	18.2	0.04
3.186539	<i>z</i>	18.19	0.05
3.206539	<i>z</i>	18.4	0.08
3.236539	<i>z</i>	18.26	0.03
3.2459	<i>z</i>	18.35	0.13
3.256539	<i>z</i>	18.23	0.03
3.276539	<i>z</i>	18.23	0.04
3.306539	<i>z</i>	18.3	0.04
3.326539	<i>z</i>	18.18	0.04
4.166539	<i>z</i>	18.63	0.05
4.186539	<i>z</i>	18.76	0.05
4.191	<i>z</i>	18.8	0.1
4.206539	<i>z</i>	18.69	0.04
4.236539	<i>z</i>	18.75	0.04
4.256539	<i>z</i>	18.74	0.05
4.276539	<i>z</i>	18.83	0.05
4.306539	<i>z</i>	18.74	0.05
4.326539	<i>z</i>	18.71	0.06
4.670249	<i>z</i>	19.21	0.02
5.7	<i>z</i>	19.39	0.05

**Note.** All times are in the observer frame. The magnitudes are not corrected for Galactic extinction.

modifications. We update the GRB-SN sample to include all GRB-SNe with an A, B, or C classification from Cano et al. (2017) and distinguish between low-luminosity GRBs in blue, high-energy jet GRBs in red, and events in the middle in gray. We plot  $L_{\gamma, \text{iso}}$  against the flux-stretching factor with respect to SN 1998bw ( $k_{\text{SN } 1998\text{bw}}$ ), along with  $M_{\text{Ni}}$ . These two parameters are both proxies for the brightness of the associated SN light curve ( $M_V$ ) that Hjorth (2013) used. We use them both in tandem as they have the additional advantage that one is a directly observable feature from the light curve ( $k_{\text{SN } 1998\text{bw}}$ ), while the other is a physical parameter derived from modeling the explosion ( $M_{\text{Ni}}$ ). We also add a few additional events to the sample of Cano et al. (2017), namely GRB 200826A/AT 2020scz (Ahumada et al. 2021) to the  $k_{\text{SN } 1998\text{bw}}$  plot, and GRB 161219B/SN 2016jca (Ashall et al. 2019) and GRB 171010A/SN 2017htp (Melandri et al. 2019) to the  $M_{\text{Ni}}$  plot. Finally, we add the results from this work to both plots, with the best-fit flux-stretching factor from Table 2,  $k_{\text{SN } 1998\text{bw}} =$

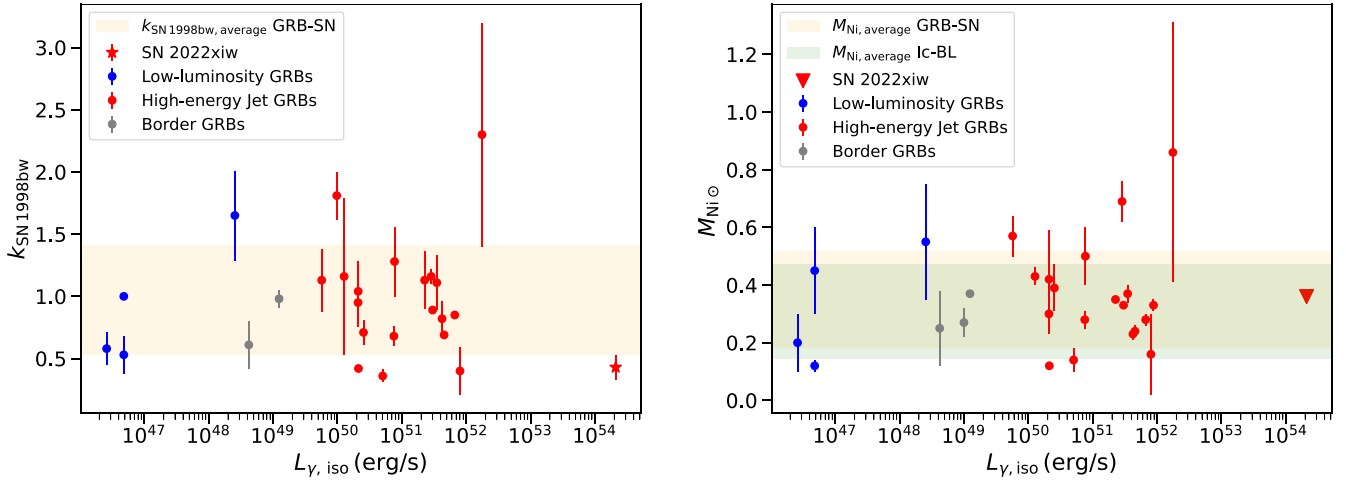


**Figure 5.** Left panel: modification of Figure 3 from Hjorth (2013), where the flux-stretching factor of the SNe with respect to SN 1998bw ( $k_{\text{SN 1998bw}}$ ) is plotted against the isotropic-equivalent  $\gamma$ -ray luminosity ( $L_{\gamma, \text{iso}}$ ) for their associated GRBs. We distinguish between low-luminosity GRBs, high-energy jet GRBs, and GRBs in the border regime. We indicate the results from this work, GRB 221009A/SN 2022xiw, with a star. We also show the average  $k_{\text{SN 1998bw}}$  for GRB-SNe in the plot with the exception of GRB 221009A/SN 2022xiw, along with its dispersion. Right panel: a similar modification of Figure 3 from Hjorth (2013), where the  $M_{\text{Ni}}$  in  $M_{\odot}$  of the SNe is plotted against the isotropic-equivalent  $\gamma$ -ray luminosity ( $L_{\gamma, \text{iso}}$ ) for their associated GRBs. We make the same distinctions between GRBs as in the above panel, and label the results from GRB 221009A/SN 2022xiw with an upper limit. We also show the average  $M_{\text{Ni}}$  and dispersion for the GRB-SNe plotted with the exception of GRB 221009A/SN 2022xiw, along with that of the Type Ic-BL sample not associated with GRBs from Taddia et al. (2019).

0.39 denoted as a star, and the limit of  $M_{\text{Ni}} < 0.36 M_{\odot}$  denoted as an upper limit.

In addition, we also plot the average  $k_{\text{SN 1998bw}}$  ( $k_{\text{SN 1998bw, average}} = 0.97$ ) and dispersion ( $\sigma = 0.44$ ) for the GRB-SNe plotted with the exception of SN 2022xiw shaded in orange, and the average  $M_{\text{Ni}}$  ( $M_{\text{Ni, average}} = 0.35 M_{\odot}$ ) and dispersion ( $\sigma = 0.17 M_{\odot}$ ) for the GRB-SNe plotted with the exception of SN 2022xiw shaded again in orange, along with for the Type Ic-BL population not associated with GRBs ( $M_{\text{Ni, average}} = 0.31 M_{\odot}$ ,  $\sigma = 0.16 M_{\odot}$ ; Taddia et al. 2019) shaded in green. From the figure, we notice that SN 2022xiw’s  $k_{\text{SN 1998bw}}$  is slightly lower than the average range for the rest of the sample, despite the burst being orders of magnitude more energetic. Furthermore, SN 2022xiw’s  $M_{\text{Ni}}$  is also likely on the lower end with respect to the overall population. The overlap between the average  $M_{\text{Ni}}$  in normal Type Ic-BL SNe and GRB-SNe suggest that there are no intrinsic differences between the brightnesses of the SNe associated with GRBs with those that are not.

We use the Pearson correlation coefficient test to determine if there are correlations between  $L_{\gamma, \text{iso}}$  and  $k_{\text{SN 1998bw}}$  and  $L_{\gamma, \text{iso}}$  and  $M_{\text{Ni}}$ , between the low-luminosity GRBs, high-energy jet GRBs, and the entire data set. In the low-luminosity regime, we do find a correlation for both  $k_{\text{SN 1998bw}}$  and  $M_{\text{Ni}}$ , with coefficients of 0.90 and 0.68, respectively. However, this correlation must be taken with caution, as there are only four low-luminosity GRBs in the sample. When testing the high-energy jet GRBs, we find no significant evidence for any correlations in the data, with coefficients of  $-0.27$  and  $0.00$  for  $k_{\text{SN 1998bw}}$  and  $M_{\text{Ni}}$ , respectively. When testing the overall data set including the border GRBs, we also find no significant evidence for any correlations, with coefficients of  $-0.22$  and  $0.01$  for  $k_{\text{SN 1998bw}}$  and  $M_{\text{Ni}}$ , respectively. These tests done on the high-energy jet GRBs and entire data set all had  $p$ -values greater than 0.25. The lack of correlations are quite interesting, especially because  $L_{\gamma, \text{iso}}$  ranges over seven orders of magnitude. This suggests that SN emission appears to be largely decoupled from any central-engine activity in GRB-SN systems.

## 6. Conclusions

By modeling the optical emission from GRB 221009A, we find moderate, but not conclusive statistical evidence ( $K_{\text{Bayes}} = 10^{1.2}$ ) for the presence of associated SN emission, and find that GRB 221009A’s associated SN 2022xiw must be substantially fainter than SN 1998bw. We also extract the physical parameters associated with the SN, assuming three different host galaxy extinction scenarios: (1)  $E(B - V)_{\text{host}}$  is allowed to vary as a free parameter between 0.3 and 0.5 mag; (2)  $E(B - V)_{\text{host}} = 0.3$  mag; and (3) there is no host galaxy extinction. The most physically plausible scenario is the first, as there is evidence for extinction larger than the nominal Schlafly & Finkbeiner (2011) value, though with a large degree of associated uncertainty (Kann et al. 2023; Levan et al. 2023; Williams et al. 2023).

We derive  $M_{\text{Ni}} = 0.05\text{--}0.25 M_{\odot}$ ,  $M_{\text{ej}} = 3.5\text{--}11.1 M_{\odot}$ , and  $E_{\text{KE}} = (1.6\text{--}5.2) \times 10^{52}$  erg. These values are weakly constrained due to the faintness of the SN emission with respect to the afterglow and host emission, but we robustly constrain an upper limit on the  $M_{\text{Ni}}$  of  $M_{\text{Ni}} < 0.36 M_{\odot}$ . All of the explosion parameters lie within the range of those found in previous GRB-SNe in the literature (Cano et al. 2017), suggesting that even the most extreme GRBs can produce SNe with explosion properties typical of the overall GRB-SN population. We investigate the explosion parameters with respect to the overall GRB-SN population, and find that there is no significant correlation between the luminosity of GRBs and their associated SN’s brightness. This suggests that central-engine activity in GRB-SN systems and SN emission are largely decoupled, and further studies in the future pinpointing why will be of utmost importance to unraveling the GRB-SN connection in totality. This event is an important addition to the GRB-SN population, and is a prime example for why it is extremely important to continue analyzing high-energy GRBs to understand further the GRB-SN connection.

G.P.S. acknowledges Geoffrey Ryan for useful discussions about Bayesian modeling techniques, as well as Mansi

Kasliwal, Kishalay De, Ryan Lau, Viraj Karambelkar, Michael Ashley, Jacob Jencson, and the Palomar Gattini Infrared Survey team for discussions about the paper during the drafting process. G.P.S. thanks James Bauer and Quanzhi Ye for their assistance obtaining the LDT observations, and Simi Bhullar for her moral support throughout the paper writing process. M. W.C. acknowledges support from the National Science Foundation with grant Nos. PHY-2010970 and OAC-2117997. R.S. acknowledges support from grant No. 12073029 from the National Natural Science Foundation of China (NSFC). J.H.G. and E.T. acknowledge support from the European Research Council (ERC) under the European Unions Horizon 2020 research and innovation program, grant 101002761. A.J.D. was supported, and M.C.M. was supported in part, by NASA ADAP grant 80NSSC21K0649. The material is based upon work supported by NASA under award No. 80GSFC21M0002.

These results made use of Lowell Observatories Lowell Discovery Telescope (LDT), formerly the Discovery Channel Telescope. Lowell operates the LDT in partnership with Boston University, Northern Arizona University, the University of Maryland, and the University of Toledo. Partial support of the LDT was provided by Discovery Communications. LMI was built by the Lowell Observatory using funds from the National Science Foundation (AST-1005313). These results were also based on observations obtained at the international Gemini Observatory, a program of NSF's NOIRLab, which is managed by the Association of Universities for Research in Astronomy (AURA) under a cooperative agreement with the National Science Foundation on behalf of the Gemini Observatory partnership: the National Science Foundation (United States), National Research Council (Canada), Agencia Nacional de Investigación y Desarrollo (Chile), Ministerio de Ciencia, Tecnología e Innovación (Argentina), Ministério da Ciência, Tecnologia, Inovações e Comunicações (Brazil), and Korea Astronomy and Space Science Institute (Republic of Korea). The GROWTH-India Telescope (GIT) is a 70 cm telescope with a 0°7 field of view, set up by the Indian Institute of Astrophysics (IIA) and the Indian Institute of Technology Bombay (IITB) with funding from Indo-US Science and Technology Forum and the Science and Engineering Research Board, Department of Science and Technology (DST), Government of India. It is located at the Indian Astronomical Observatory (Hanle), operated by IIA an autonomous institute under DST. We acknowledge funding by the IITB alumni batch of 1994, which partially supports operations of the telescope.

*Facilities:* Lowell Discovery Telescope (LDT), GROWTH-India Telescope (GIT), Gemini-South Telescope.

*Software:* PYMULTINEST (Feroz et al. 2009; Buchner et al. 2014); ASTROPY (Astropy Collaboration et al. 2013); EMCEE (Foreman-Mackey et al. 2013).

### ORCID iDs

Gokul P. Srinivasaragavan  <https://orcid.org/0000-0002-6428-2700>


Brendan O'Connor  <https://orcid.org/0000-0002-9700-0036>

S. Bradley Cenko  <https://orcid.org/0000-0003-1673-970X>

Alexander J. Dittmann  <https://orcid.org/0000-0001-6157-6722>

Sheng Yang  <https://orcid.org/0000-0002-2898-6532>

Jesper Sollerman  <https://orcid.org/0000-0003-1546-6615>

G. C. Anupama  <https://orcid.org/0000-0003-3533-7183>  
 Sudhanshu Barway  <https://orcid.org/0000-0002-3927-5402>  
 Varun Bhalerao  <https://orcid.org/0000-0002-6112-7609>  
 Harsh Kumar  <https://orcid.org/0000-0003-0871-4641>  
 Vishwajeet Swain  <https://orcid.org/0000-0002-7942-8477>  
 Erica Hammerstein  <https://orcid.org/0000-0002-5698-8703>  
 Isiah Holt  <https://orcid.org/0000-0002-3097-942X>  
 Shreya Anand  <https://orcid.org/0000-0003-3768-7515>  
 Igor Andreoni  <https://orcid.org/0000-0002-8977-1498>  
 Michael W. Coughlin  <https://orcid.org/0000-0002-8262-2924>  
 Simone Dichiarà  <https://orcid.org/0000-0001-6849-1270>  
 Avishay Gal-Yam  <https://orcid.org/0000-0002-3653-5598>  
 M. Coleman Miller  <https://orcid.org/0000-0002-2666-728X>  
 Jaime Soon  <https://orcid.org/0000-0001-9226-4043>  
 Roberto Soria  <https://orcid.org/0000-0002-4622-796X>  
 Joseph Durbak  <https://orcid.org/0000-0002-3774-1270>  
 James H. Gillanders  <https://orcid.org/0000-0002-8094-6108>  
 Sibasish Laha  <https://orcid.org/0000-0003-2714-0487>  
 Anna M. Moore  <https://orcid.org/0000-0002-2894-6936>  
 Fabio Ragosta  <https://orcid.org/0000-0003-2132-3610>  
 Eleonora Troja  <https://orcid.org/0000-0002-1869-7817>

### References

- Ahumada, T., Singer, L. P., Anand, S., et al. 2021, *NatAs*, 5, 917  
 Arnett, W. D. 1982, *ApJ*, 253, 785  
 Ashall, C., Mazzali, P. A., Pian, E., et al. 2019, *MNRAS*, 487, 5824  
 Astropy Collaboration, Robitaille, T. P., Tollerud, E. J., et al. 2013, *A&A*, 558, A33  
 Barbary, K., Barclay, T., Biswas, R., et al. 2016, SNCosmo: Python library for supernova cosmology, Astrophysics Source Code Library, ascl:1611.017  
 Barthelmy, S. D., Barbier, L. M., Cummings, J. R., et al. 2005, *SSRv*, 120, 143  
 Belkin, S., Kim, V., Pozanenko, A., et al. 2022a, *GCN*, 32769, 1  
 Belkin, S., Moskvitin, A., Kim, V., et al. 2022b, *GCN*, 32818, 1  
 Belkin, S., Nazarov, S., Pozanenko, A., Pankov, N. & IKI GRB FuN 2022, *GCN*, 32684, 1  
 Bertin, E. 2010, SWarp: Resampling and Co-adding FITS Images Together, Astrophysics Source Code Library, ascl:1010.068  
 Bertin, E., & Arnouts, S. 1996, *A&AS*, 117, 393  
 Bikmaev, I., Khamitov, I., Irtuganov, E., et al. 2022a, *GCN*, 32743, 1  
 Bikmaev, I., Khamitov, I., Irtuganov, E., et al. 2022b, *GCN*, 32752, 1  
 Brivio, R., Ferro, M., D'Avanzo, P., et al. 2022, *GCN*, 32652, 1  
 Buchner, J., Georgakakis, A., Nandra, K., et al. 2014, *A&A*, 564, A125  
 Burns, E., Svinkin, D., Fenimore, E., et al. 2023, *ApJL*, 946, L31  
 Cano, Z., Wang, S.-Q., Dai, Z.-G., & Wu, X.-F. 2017, *AdAst*, 2017, 8929054  
 Cardelli, J. A., Clayton, G. C., & Mathis, J. S. 1989, *ApJ*, 345, 245  
 Castro-Tirado, A. J., Sanchez-Ramirez, R., Hu, Y. D., et al. 2022, *GCN*, 32686, 1  
 Clocciatti, A., Suntzeff, N. B., Covarrubias, R., & Candia, P. 2011, *AJ*, 141, 163  
 Corsi, A., Gal-Yam, A., Kulkarni, S. R., et al. 2016, *ApJ*, 830, 42  
 Corsi, A., Ho, A. Y. Q., Cenko, S. B., et al. 2022, arXiv:2210.09536  
 D'Avanzo, P., Ferro, M., Brivio, R., et al. 2022, *GCN*, 32755, 1  
 de Ugarte Postigo, A., Izzo, L., Pugliese, G., et al. 2022a, *GCN*, 32648, 1  
 de Ugarte Postigo, A., Izzo, L., Thoene, C. C., et al. 2022b, *GCN*, 32800, 1  
 de Ugarte Postigo, A., Izzo, L., Thoene, C. C., et al. 2022c, *TNSCR*, 2022-3047, 1  
 de Wet, S., Groot, P. J. & Meerlicht Consortium 2022, *GCN*, 32646, 1  
 D'Elia, V., Pian, E., Melandri, A., et al. 2015, *A&A*, 577, A116  
 Dichiarà, S., Gropp, J. D., Kennea, J. A., et al. 2022, *GCN*, 32632, 1  
 Feroz, F., Hobson, M. P., & Bridges, M. 2009, *MNRAS*, 398, 1601  
 Ferro, M., Brivio, R., D'Avanzo, P., et al. 2022, *GCN*, 32804, 1  
 Filippenko, A. V. 1997, *ARA&A*, 35, 309  
 Flewelling, H. A., Magnier, E. A., Chambers, K. C., et al. 2020, *ApJS*, 251, 7  
 Foreman-Mackey, D., Hogg, D. W., Lang, D., & Goodman, J. 2013, *PASP*, 125, 306  
 Frederiks, D., Svinkin, D., Lysenko, A. L., et al. 2023, arXiv:2302.13383  
 Fulton, M. D., Smartt, S. J., Rhodes, L., et al. 2023, *ApJL*, 946, L22  
 Gehrels, N., Chincarini, G., Giommi, P., et al. 2004, *ApJ*, 611, 1005  
 Groot, P. J., Vreeswijk, P. M., Ter Horst, R., et al. 2022, *GCN*, 32678, 1

- Gupta, R., Ror, A. K., Pandey, S. B., et al. 2022, GCN, [32811](#), 1
- Hjorth, J. 2013, [RSPTA](#), [371](#), [20120275](#)
- Huber, M., Schultz, A., Chambers, K. C., et al. 2022, GCN, [32758](#), 1
- Im, M., Paek, G. S. H., Lim, G., et al. 2022, GCN, [32803](#), 1
- Iwamoto, K., Mazzali, P. A., Nomoto, K., et al. 1998, [Natur](#), [395](#), [672](#)
- Izzo, L., Saccardi, A., Fynbo, J. P. U., et al. 2022, GCN, [32765](#), 1
- Jakobsson, P., Levan, A., Fynbo, J. P. U., et al. 2006, [A&A](#), [447](#), [897](#)
- Jester, S., Schneider, D. P., Richards, G. T., et al. 2005, [AJ](#), [130](#), [873](#)
- Kann, D. A., Agayeva, S., Aivazyan, V., et al. 2023, [ApJL](#), [948](#), [L12](#)
- Kann, D. A., Masetti, N., & Klose, S. 2007, [AJ](#), [133](#), [1187](#)
- Kim, V., Krugov, M., Pozanenko, A., et al. 2022, GCN, [32670](#), 1
- Klose, S., Schmidl, S., Kann, D. A., et al. 2019, [A&A](#), [622](#), [A138](#)
- Kumar, H., Bhalerao, V., Anupama, G. C., et al. 2022b, [AJ](#), [164](#), [90](#)
- Kumar, H., Bhalerao, V., Anupama, G. C., et al. 2022c, [MNRAS](#), [516](#), [4517](#)
- Kumar, H., Swain, V., Waratkar, G., et al. 2022a, GCN, [32662](#), 1
- Labrie, K., Anderson, K., Cárdenes, R., Simpson, C., & Turner, J. E. H. 2019, in ASP Conf. Ser. 523, *Astronomical Data Analysis Software and Systems XXVIII*, ed. M. W. Teuben et al. (San Francisco, CA: ASP), [321](#)
- Laskar, T., Alexander, K. D., Ayache, E., et al. 2022, GCN, [32757](#), 1
- Laskar, T., Alexander, K. D., Margutti, R., et al. 2023, [ApJL](#), [946](#), [L23](#)
- Lesage, S., Veres, P., Roberts, O. J., et al. 2022, GCN, [32642](#), 1
- Levan, A. J., Lamb, G. P., Schneider, B., et al. 2023, [ApJL](#), [946](#), [L28](#)
- Lyman, J. D., Bersier, D., & James, P. A. 2014, [MNRAS](#), [437](#), [3848](#)
- Lyman, J. D., Bersier, D., James, P. A., et al. 2016, [MNRAS](#), [457](#), [328](#)
- Malesani, D. B., Levan, A. J., Izzo, L., et al. 2023, arXiv:[2302.07891](#)
- McCully, C., & Tewes, M. 2019, *Astro-SCRAPPY: Speedy Cosmic Ray Annihilation Package in Python*, *Astrophysics Source Code Library*, ascl:[1907.032](#)
- Meegan, C., Lichti, G., Bhat, P. N., et al. 2009, [ApJ](#), [702](#), [791](#)
- Melandri, A., Malesani, D. B., Izzo, L., et al. 2019, [MNRAS](#), [490](#), [5366](#)
- Mészáros, P., & Rees, M. J. 1997, [ApJ](#), [476](#), [232](#)
- Oates, S. R., Page, M. J., Schady, P., et al. 2009, [MNRAS](#), [395](#), [490](#)
- O'Connor, B., Cenko, S. B., Troja, E., et al. 2022a, GCN, [32739](#), 1
- O'Connor, B., Cenko, S. B., Troja, E., et al. 2022b, GCN, [32799](#), 1
- O'Connor, B., Troja, E., Ryan, G., et al. 2023, arXiv:[2302.07906](#)
- Pellegrin, K., Rumstay, K., & Hartmann, D. 2022, GCN, [32852](#), 1
- Rajabov, Y., Sadibekova, T., Tillayev, Y., et al. 2022, GCN, [32795](#), 1
- Rastinejad, J., & Fong, W. 2022, GCN, [32749](#), 1
- Rossi, A., Maiorano, E., Malesani, D. B., et al. 2022, GCN, [32809](#), 1
- Sari, R., Piran, T., & Narayan, R. 1998, [ApJL](#), [497](#), [L17](#)
- Schlafly, E. F., & Finkbeiner, D. P. 2011, [ApJ](#), [737](#), [103](#)
- Schneider, B., Adami, C., Le Floch, E., et al. 2022, GCN, [32753](#), 1
- Shrestha, M., Bostroem, K., Sand, D., et al. 2022, GCN, [32771](#), 1
- Shrestha, M., Sand, D. J., Alexander, K. D., et al. 2023, [ApJL](#), [946](#), [L25](#)
- Soderberg, A. M., Nakar, E., Berger, E., & Kulkarni, S. R. 2006, [ApJ](#), [638](#), [930](#)
- Sollerman, J., Kozma, C., Fransson, C., et al. 2000, [ApJL](#), [537](#), [L127](#)
- Stritzinger, M. D., Hamuy, M., Suntzeff, N. B., et al. 2002, *AAS Meeting Abstracts*, [200](#), [95.03](#)
- Taddia, F., Sollerman, J., Fremling, C., et al. 2019, [A&A](#), [621](#), [A71](#)
- Taddia, F., Stritzinger, M. D., Bersten, M., et al. 2018, [A&A](#), [609](#), [A136](#)
- Tiengo, A., Pintore, F., Vaia, B., et al. 2023, [ApJL](#), [946](#), [L30](#)
- Toy, V. L., Cenko, S. B., Silverman, J. M., et al. 2016, [ApJ](#), [818](#), [79](#)
- Trotta, R. 2008, [ConPh](#), [49](#), [71](#)
- Valenti, S., Benetti, S., Cappellaro, E., et al. 2008, [MNRAS](#), [383](#), [1485](#)
- Vinko, J., Bodi, A., Pal, A., et al. 2022, GCN, [32709](#), 1
- Williams, M. A., Kennea, J. A., Dichiara, S., et al. 2023, [ApJL](#), [946](#), [L24](#)
- Woosley, S. E., & Bloom, J. S. 2006, [ARA&A](#), [44](#), [507](#)
- Yang, S., & Sollerman, J. 2023, arXiv:[2302.02082](#)